ACS APPLIED MATERIALS & INTERFACES

Research Article

www.acsami.org

Spin-Glass-Like Behavior and Topological Hall Effect in $SrRuO_3/SrIrO_3$ Superlattices for Oxide Spintronics Applications

Bin Pang,[†] Lunyong Zhang,*[,†,‡] Y. B. Chen,*[,§] Jian Zhou,[†] Shuhua Yao,[†] Shantao Zhang,[†] and Yanfeng Chen[†]

[†]National Laboratory of Solid State Microstructures & Department of Materials Science and Engineering, Nanjing University, Nanjing 210093, China

[‡]Max Planck POSTECH Center for Complex Phase Materials, Max Planck POSTECH/Korea Research Initiative (MPK), Gyeongbuk 376-73, Korea

[§]National Laboratory of Solid State Microstructures & Department of Physics, Nanjing University, 210093 Nanjing, China

Supporting Information

ABSTRACT: The heterostructure interface provides a powerful platform for exploring rich emergent phenomena, such as interfacial superconductivity and nontrivial topological surface states. Here, $SrRuO_3/SrIrO_3$ superlattices were epitaxially synthesized. The magnetic and magneto-transport properties of these superlattices were characterized. A broad cusp-type splitting in the zero-field-cooling/field-cooling temperature-dependent magnetization and magnetization relaxation, which follows the modified stretched function model, accompanied by double hysteresis magnetization loops were demonstrated. These physical effects were modulated by the $SrIrO_3$ layer thickness, which confirms the coexistence of interfacial spin glass and ferromagnetic ordering in the superlattices. In addition, the topological Hall effect was observed at low temperatures, and it is weakened with the increase of the $SrIrO_3$ layer thickness. These results suggest that a noncoplanar spin texture is generated at the $SrRuO_3/SrIrO_3$ interfaces because of the interfacial Dzyaloshinskii–Moriya interaction. This work demonstrates that $SrIrO_3$ can effectively induce interfacial Dzyaloshinskii–Moriya interactions in superlattices, which would serve as a mechanism to develop spintronic devices with perovskite oxides.

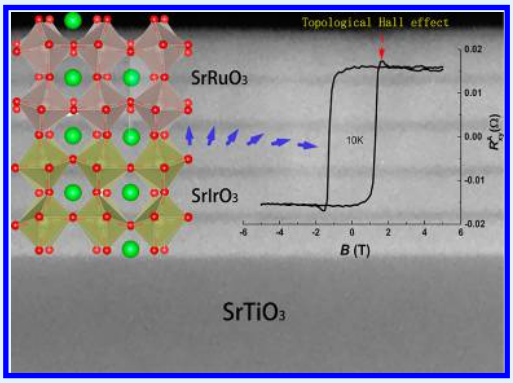

KEYWORDS: *spin–orbit interaction, superlattices, spin glass, topological Hall effect, noncoplanar spin ordering, Dzyaloshinskii–Moriya interaction*

I. INTRODUCTION

Perovskite compounds with spin–orbit interactions (SOI), for example, the $Sr_{n+1}Ir_nO_{3n+1}$ oxides, have been extensively studied in recent years, as their SOI intensity is comparable to that of crystal field splitting and electron–electron interactions. Accordingly, the insulating antiferromagnetic Sr_2IrO_4 is described as a new type of spin–orbit interaction assistant Mott insulator.[1] Metastable orthorhombic $SrIrO_3$ (SIO), as a three-dimensional sister compound of Sr_2IrO_4, has also attracted significant attention from the materials and physics community. The first-principles and effective Hamiltonian methods predict that heterostructures composed of SIO and other ABO_3-type perovskite compounds are potential candidates for topological insulators.[2,3] In addition to these predicted topological states, heterostructures composed of SIO and other compounds exhibit a series of magnetism-modulated functionalities. For example, the magnetic easy axis in $La_{2/3}Sr_{1/3}MnO_3$/SIO superlattice is controlled by the thickness of SIO.[4] The canted antiferromagnetic ordering in SIO can be induced in the $SIO/SrTiO_3$ superlattice when the thickness of SIO is lower than 4 unit cells,[5] though the bulk SIO is paramagnetic. Our previous work validated that orthorhombic $SrIrO_3$ can be synthesized as a film by pulsed laser deposition.[6] The analysis of the magnetoresistance demonstrates that there is a very large SOI in the SIO thin films.[7] It has been reported that a large SOI can induce Dzyaloshinskii–Moriya interactions (DMIs) at heterostructure interfaces.[8,9] If we synthesize SIO with a ferromagnetic oxide, such as $SrRuO_3$ (SRO), the interfacial DMI will conceptually induce a noncollinear/noncoplanar spin texture in $SrRuO_3$, which might demonstrate some novel functionalities. By taking this into consideration, here, we intentionally synthesized superlattices composed of varied-thickness SIO layers with SRO layers (fixed as 4 nm). A spin-glass-like state and the topological Hall effect were observed, and they can be reasonably attributed to the formation of noncoplanar spin textures at the SIO/SRO interfaces under DMIs. Our work demonstrates that a novel functionality can be realized in heterostructures composed of $SrIrO_3$ and other

Received: January 4, 2017
Accepted: January 6, 2017
Published: January 6, 2017

DOI: 10.1021/acsami.7b00150
ACS Appl. Mater. Interfaces 2017, 9, 3201–3207

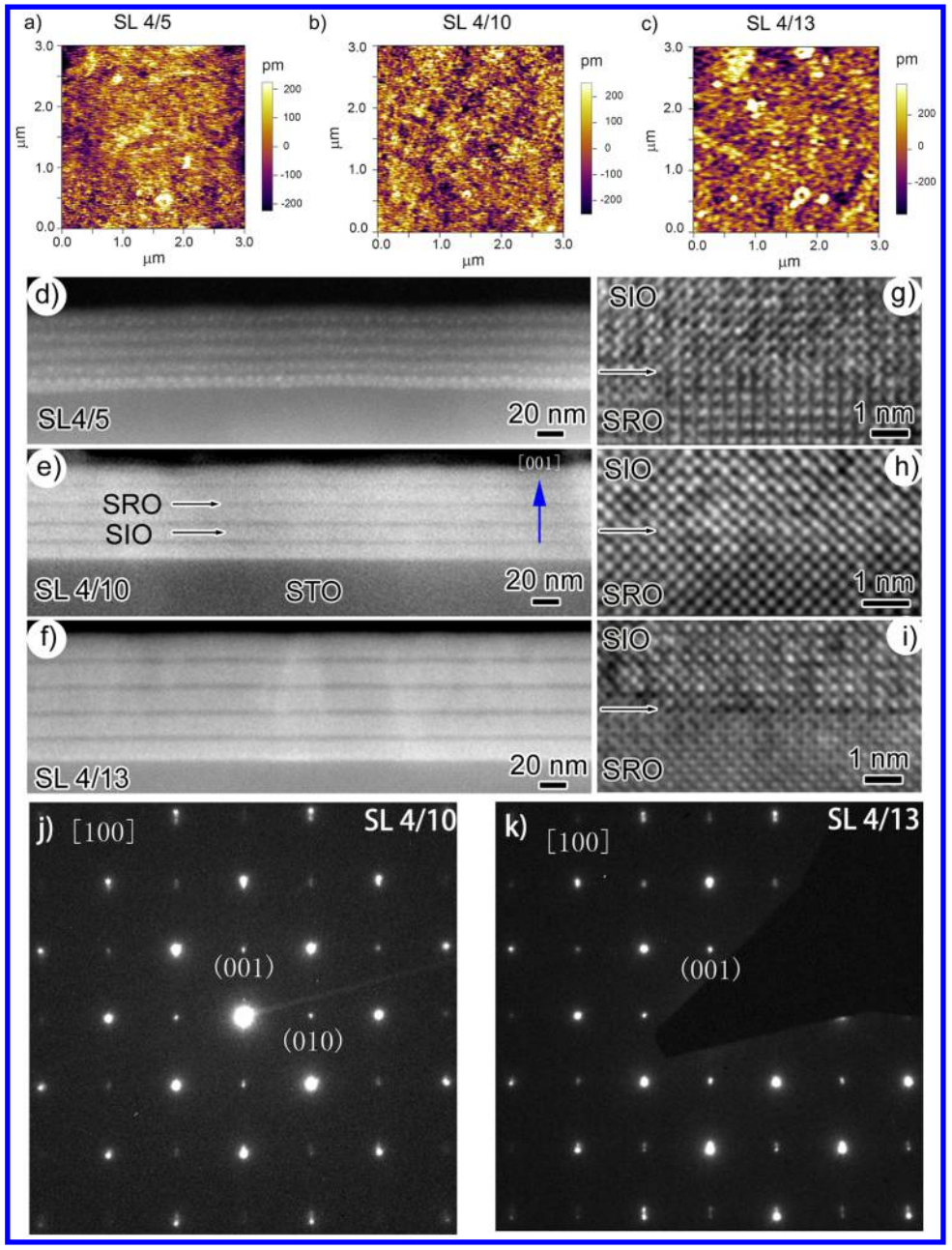

Figure 1. (a–c) Atomic force microscopy images of the superlattices showing the two-dimensional growth model terrace surfaces; (d–f and g–i) TEM contrast images and HRTEM patterns of the superlattice samples, respectively, illustrating the clear flat interfaces; (j and k) SAED patterns of the SL4/10 and SL4/13 superlattices.

perovskite oxides, and it presents the experimental evidence of SOIs, which participate in the interfacial coupling between 5d and other functional materials. In particular, it expands the current research interest in the strong SOI of 5d transition metal oxides to the area of interfacial engineering, which paves the way toward achieving all-oxide spintronics applications.

II. EXPERIMENTAL SECTION

Three superlattices were grown, with 4 nm-SRO/thickness-varied SIO on chemically etched flat (001)-$SrTiO_3$ substrates with TiO_2-termination on the surface,[10] by a pulse laser deposition system (PLD, AdNaNo) at a repetition rate of 2 Hz repetition, a substrate temperature of 800 °C and in a 75 mTorr oxygen atmosphere. The SIO layer thicknesses in the three samples are approximately 5, 10, and 13 nm; hereafter, these three samples are labeled as SL4/5, SL4/10, and SL4/13, respectively. The thicknesses of these samples were also measured by transmission electron microscopy (TEM, Tecnai F20, FEI Inc.). All the characterizations of the magnetic properties were carried out in a Quantum Design Magnetic Property Measurement System (MPMS3-SQUID), and all the electron transport measurements were performed using the standard four-probe method in a 9T-Quantum Design Physical Property Measurement System (PPMS). The surface morphology was characterized by an Asylum Cypher atomic force microscopy system. For the magnetization relaxation experiments, two types of measurements were adopted. In one measurement, the samples were 0.1 T field cooled to the target temperature from room temperature; then, the field was removed, and the magnetization data (denoted here as R_{FC})

DOI: 10.1021/acsami.7b00150
ACS Appl. Mater. Interfaces 2017, 9, 3201–3207

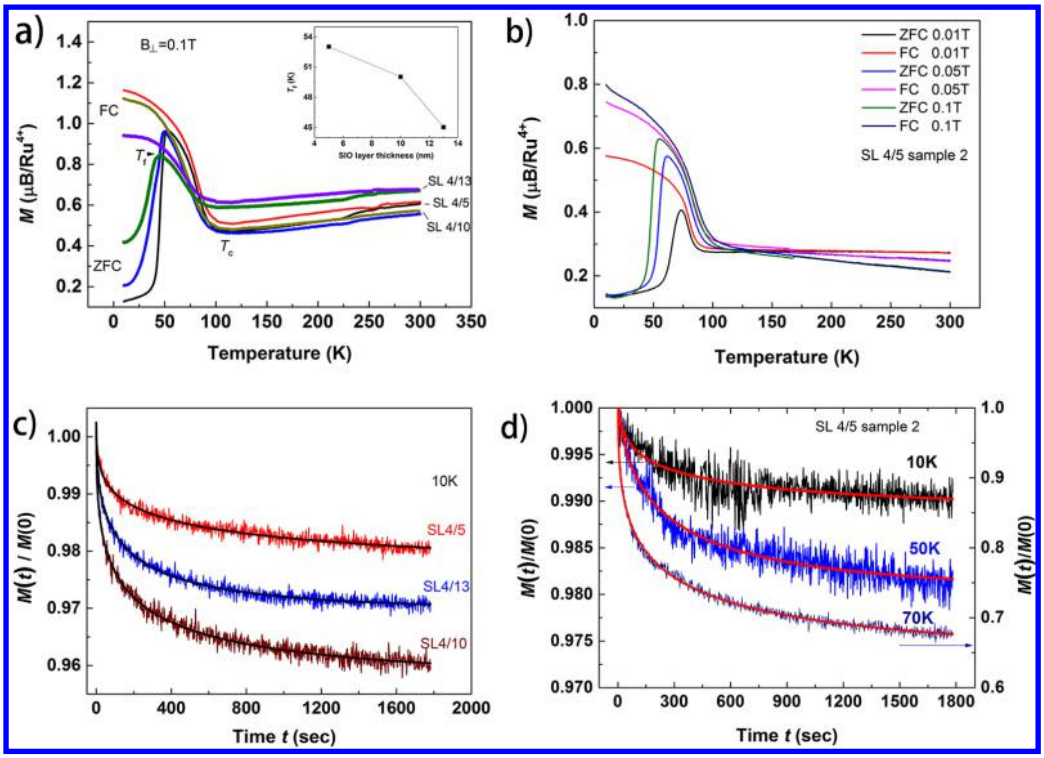

Figure 2. Magnetic behaviors of the superlattices. (a) Temperature-dependent magnetization curves (ZFC and FC) of the samples; the inset shows the SIO layer thickness dependence of the spin-glass freezing temperature T_f. (b) Temperature-dependent magnetization curves of a SL 4/5 sample under a difference magnetic field. (c) The magnetization relaxation curves of the samples at 10 K under the R_{ZFC} measurement route. (d) The magnetization relaxation curves of a SL 4/5 sample under the R_{FC} measurement route at varied temperatures. The relaxation data were fitted using the modified stretched function model, which are shown as the solid curves.

were subsequently collected. In the second measurement, the samples were first zero-field cooled to the target temperature and then kept in an out-of-plane magnetic field of 0.1 T for 5 min; afterward, the field was removed, the magnetization data (denoted as R_{ZFC}) were collected. The second measurement is crucial to distinguish the long-range magnetic order state and the spin-glass-like state (see the Supporting Information for details).

III. RESULTS

Figure 1a−1c presents the surface morphologies of the samples, where two-dimensional growth model terraces are demonstrated, which is consistent with the distinct flat interfaces observed from the high-angle annular dark field images and the high-resolution TEM (HRTEM) images, as observed in Figure 1d−1i, which indicates that there is no obvious atomic diffusion at the interfaces. The X-ray diffraction (XRD) patterns exhibit distinct superlattice satellite peaks (Figure S2). Therefore, it can be concluded that high-quality superlattices were successfully synthesized, and no obvious structural differences are observed among the three series samples, except for the layer thickness of SIO (as observed from the XRD patterns and HRTEM). The orthorhombic structures of the SRO and the SIO layers were initially confirmed by the XRD patterns (Figure S2) and further verified by the selected area electron diffraction (SAED) patterns shown in Figure 1j and 1k; only a slight peak splitting can be distinguished at the high-index reflections.[6] These characterizations confirm that the SRO/SIO superlattices are epitaxially constrained.

Figure 2a demonstrates the temperature-dependent magnetization under zero-field cooling (ZFC) and 0.1 T field cooling (FC, where the field was aligned perpendicular to the surface plane) conditions. Clearly, for all the samples, a sharply increasing magnetization that begins at approximately 100 K is revealed on both the ZFC and FC curves, which corresponds to the itinerant ferromagnetic transition of the $SrRuO_3$ layers. The Curie temperature T_c measured in the superlattices is lower than that of bulk $SrRuO_3$ by approximately 50−60 K, which is attributed to the strain effect in epitaxial SRO thin films.[11]

At some lower temperatures, broad cusps splitting of the FC and ZFC curves are observed for all the samples. T_f, which represents the peak temperature of the ZFC curves, decreases with the increase of the SIO layer thickness and the magnetic field applied in the magnetization measurements (Figure 2a and 2b, respectively). Such a broad splitting may be attributed to spin-glass-like behavior. We then characterized the magnetization relaxation behavior in these samples. The magnetization relaxation curves of these samples at 10 K using the R_{ZFC} measurement route and the magnetization relaxation curves of an SL 4/5 sample using the R_{FC} measurement route at varying temperatures are shown in Figure 2c and 2d, respectively. One observes that the magnetizations decay rapidly and then saturate to a constant value. Quantitatively, the magnetization relaxation dynamics at the spin-glass freezing temperature regime cannot be well fitted using the pure Stretched function $M(t) \sim \exp[-(t/\tau)^{\alpha}]$, which is usually observed in simple spin-glass systems[12] (see section III in the Supporting Information), but it can be accurately tracked with a modified Stretched function model[13,14] by adding a constant M_0, that is, $M(t) = M_0 + M_1 \exp[-(t/\tau)^{\alpha}]$, as indicated by the solid lines in Figure 2c and 2d. τ is the time constant, and M_0 and M_1 are constants. α is a constant ranging from 0 to 1. It can be observed that the

DOI: 10.1021/acsami.7b00150
ACS Appl. Mater. Interfaces 2017, 9, 3201−3207

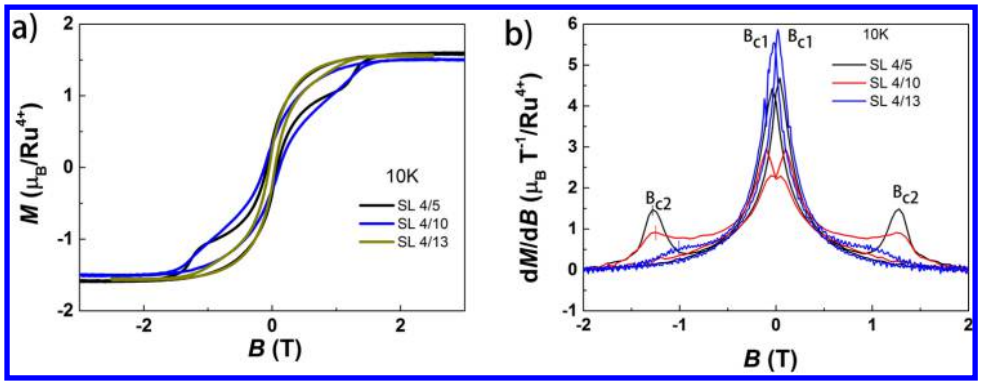

Figure 3. (a) Magnetic hysteresis loops of the samples. Two-step magnetization behaviors were demonstrated, suggesting that the spins undergo two switching processes. (b) Differential of the magnetization with respect to the field. The vertical short lines mark the peak points (B_{c2}).

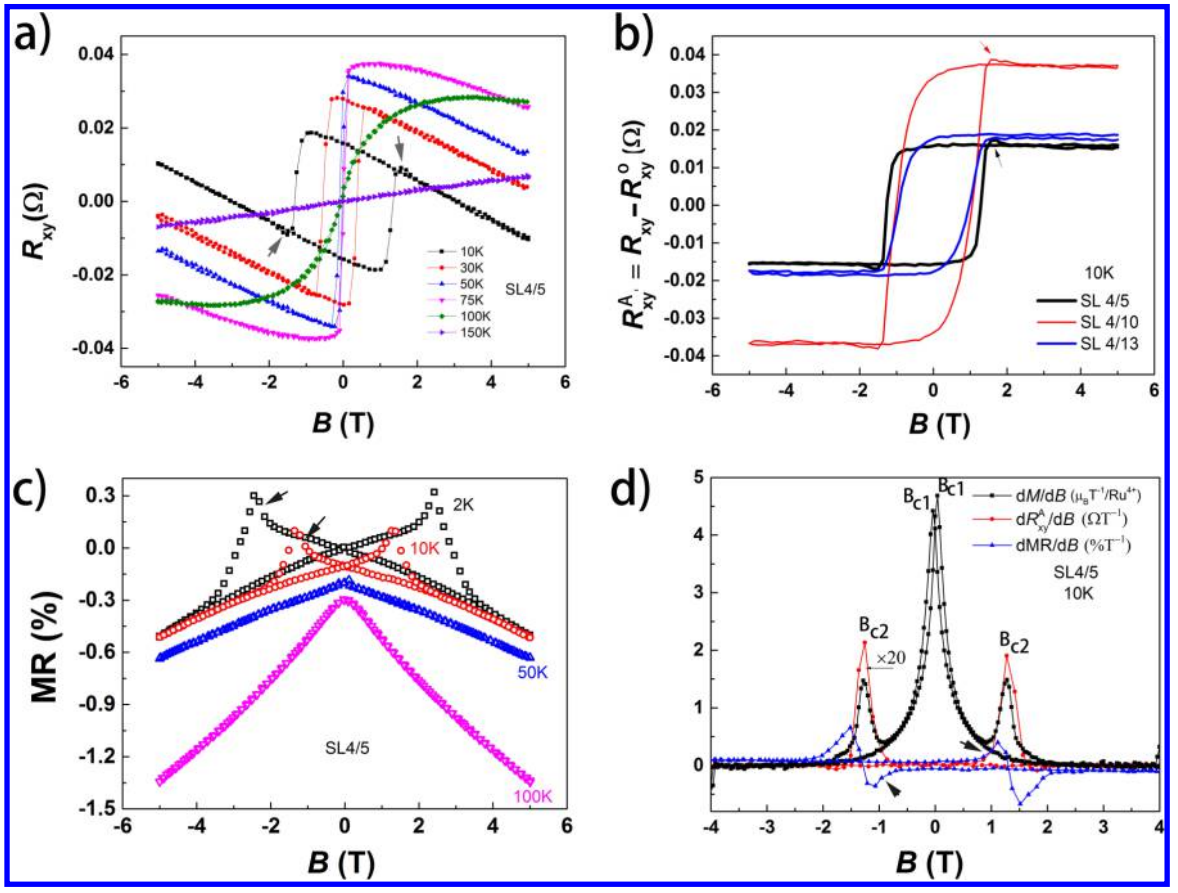

Figure 4. Electron transport behaviors of the superlattices. (a) Hall resistances of the SL 4/5 sample at varied temperatures; the arrows highlight the THE signal shown on the 10 K trace. (b) Hall resistances subtracted from the ordinary Hall resistance components of the samples at 10 K. (c) Magnetoresistances of the SL 4/5 sample; the arrows highlight the abrupt increase in MR induced by the recovering of the chiral ordering spin texture on the 2K and 10K traces. The data of the 10K, 50K and 100 K have been intentionally shifted by −0.1%, −0.2%, and −0.3%, respectively for visual clarity. Basically the MR is zero at zero-field for all the temperatures. (d) Differentials of the magnetization, the Hall resistance and the magnetoresistance of the SL 4/5 sample, which demonstrate the field correspondence of their peaks.

experimental data can be accurately fitted using this empirical equation. The fitted parameters are listed in Table S1. The constant M_0 is interpreted as the ferromagnetic (FM) contribution in the Gabay-Toulouse model, which proves that spin glass can coexist with long-range FM ordering.[15] As the SRO layer is ferromagnetic, it is reasonably deduced that our superlattice samples have a spin-glass-like state that coexists with the ferromagnetic background.

From Figure 2d, it is observed that $M(t)/M(0)$ increases as the temperature decreases, which indicates that the magnetization relaxed slower at lower temperatures. This is a normal relaxation behavior, which is attributed to the weakening of the thermally activated spin orientation fluctuation and the enhancement of the domain wall pinning effect as the temperature decreases. Figure 2c demonstrates that the $M(t)/M(0)$ has the following tendency: SL 4/5 > SL 4/13 > SL 4/10, and the mechanism for this is more complicated, thus, it will be discussed at the end of the next section.

The magnetization loop ($M-B$) measurements (see Figure 3a) show plateau-like magnetization curves in all the samples, in

DOI: 10.1021/acsami.7b00150
ACS Appl. Mater. Interfaces 2017, 9, 3201−3207

contrast to the single-step hysteresis loop in pure $SrRuO_3$ thin films grown on a (001)-$SrTiO_3$ substrate.[16,17] The corresponding differential curves dM/dB over B are plotted in Figure 3b. One can see two groups of peaks. The peaks at a low field correspond to a coercive field (B_{c1}) of the first magnetization plateau, and those at a high field (B_{c2}) represent the second magnetization plateau. B_{c1} is smaller than ∼0.5T which is at the same magnitude with that always indicated in $SrRuO_3$ films.[16,17] Conversely, B_{c2} is larger than 1T. Remarkably, B_{c1} is insensitive to the thickness of the SIO layer, while B_{c2} is strongly dependent on the SIO-layer thickness. For example, B_{c2} is nearly indistinguishable in the SL4/13 sample. In company with the magnitude of B_{c1} and $B_{c2,}$ this suggests that B_{c1} is caused by the SRO layer because the thickness of the SRO layer is fixed in all samples, while B_{c2} is related to the SIO layer. The plateau-like behavior can be related to the switching of the FM background and the spin-glass textures in the superlattices. Therefore, the $M-B$ curves also support the coexistence of spin glass and the FM background in the samples. It should be emphasized that the spin-glass-like behavior is generated at the interfaces because the second magnetization plateau is weakened and B_{c2} decreases with the increase of the SIO-layer thickness.

The magneto-transport properties of these samples were also characterized. Figure 4a typically represents the Hall traces of one SL 4/5 sample at different temperature regimes, a good square-shaped opened hysteresis with a magnetization-related anomalous Hall effect is distinct at the magnetic states (T < 100 K), which is universally observed in bulk $SrRuO_3$.[18] Particularly, peaks of R_{xy} (highlighted by the arrows) appear on the 10K Hall curve, which has never been observed in the $SrRuO_3$ system.[18] More clearly, an emergent part of R_{xy} at 10K for the samples, after the removal of the ordinary Hall portion ($R^{A}_{xy} = R_{xy} - R^{\circ}_{xy}$), is shown in Figure 4b. Moreover, the magnetic fields of the emergent peaks in $R_{xy}-B$ are identical to the B_{c2} field in the M-B curves. This suggests that they originate from the same mechanism (Figure 4d). A similar emergent behavior has been previously reported in some systems, such as in the itinerant-electron magnet MnSi,[19,20] the centrosymmetric EuO thin films[21] and the magnetic/nonmagnetic topological insulator heterostructures, $Cr_x(Bi_{1-y}Sb_y)_{2-x}Te_3/(Bi_{1-y}Sb_y)_2Te_3$.[22] This type of anomalous Hall effect is denoted as the topological Hall effect (THE) in these systems, and it is attributed to the noncoplanar spin structure. Our results therefore reasonably suggest that the THE, and so the noncoplanar spin structure were generated in our samples. Furthermore, we note that the THE signal is weakened in the SL 4/10 samples, and it disappeared in the SL 4/13 samples (Figure 4b), which illustrates that the interfaces play a fundamental role in producing the THE.

The magnetoresistance, which is defined as MR = $[R - R(B = 0)]/R(B = 0)$, could also provide evidence of the spin structure. The MR curves shown in Figure 4c and Figure S8a and S8b further reveal the strong correlation between charge transport and the spin structure. The MR curves of the SL 4/5 sample, measured at 2 and 10 K, show a typical butterfly like feature. An unusual feature in Figure 4c is the abruptly sharp increase of MR, which is highlighted by the arrows on the 2 and 10 K curves. It is distinctly different from the round MR peak always seen in $SrRuO_3$ films.[23] This feature is more clearly revealed by the dMR/dB as additional peaks, which are indicated by the arrows in Figure 4d. Figure S8 further shows that this feature vanishes in the SL 4/10 and SL 4/13 samples. Comparing the dMR/dB, dM/dB and dR^{A}_{xy}/dB curves shown in Figure 4d, the magnetic field of the MR maximum in the SL 4/5 sample is obviously identical to the B_{c2} peaks of dM/dB and dR^{A}_{xy}/dB, which suggests that the unusually sharp increase of MR originated from the same mechanism as that of the second magnetization plateau and the THE. They are attributed to the interfacial DMI, which induces a noncoplanar spin texture at the superlattice interfaces. It is also demonstrated in Figure 4a and 4c that B_{c2} is enhanced as the temperature decreases, which indicates that larger driving forces are needed to rotate and align the spin moments in the noncoplanar spin texture at lower temperatures. The relevant mechanism is the same as that stated above for the temperature-dependent $M(t)/M(0)$ profile for the SL 4/5 sample, as shown in Figure 2d. As the temperature decreases, the thermally activated spin orientation fluctuation decreases, the pinning of the magnetic domain increases, and consequently the coercive field increases.

IV. DISCUSSION

Traditionally, the alternating current susceptibility measurement (AC-χ) is an important method used to reveal the spin-glass state in most cases. We have tried to measure the AC-χ of the samples; however, unfortunately, a distinct AC-χ peak relevant to the spin glass was not observed since the magnetic signal in the superlattice films is too weak and is thus hidden by the background noise of the SQUID. Nevertheless, a spin-glass-like state is presumably the most reasonable conclusion drawn from the five experimental results demonstrated above: (1) the broad cusp-type splitting between the FC-ZFC magnetization curves, (2) the broad cusp peak temperature in the ZFC curve reduces as the external magnetic field increases, (3) a distinct magnetization relaxation, (4) a magnetization loop with hysteresis, which rules out the superparamagnetic state, and (5) the THE that indicates a noncoplanar spin structure, which is expected to induce spin-glass behaviors.[24,25]

Next, we would like to discuss the possible underlying mechanism for the observed spin-glass-like state and the THE. First, we would like to rule out the possibility of the generation of ferromagnetism in the SIO layers. In Figure S8, the magnetization of a 4 nm SIO single-layer film is nearly negligible within the resolution of our SQUID. This conclusion is also in agreement with ref 5, which claimed that SIO is paramagnetic when its thickness is larger than 4 unit cells (∼1.6 nm). Second, what is the role of the SIO layer in the abnormal magnetic behavior observed in the SRO/SIO superlattices? According to above-mentioned data, the abnormal SIO-thickness-dependent magnetic behavior should come from the interfacial effect. Considering the large SOI in SIO, the most possible candidate is the induced DMI at the non-inversion symmetric interfaces, similar to the discoveries in recent years that a noticeable interfacial DMI can be induced in multilayers constructed from an ultrathin FM layer and a nonmagnetic heavy metal with a strong SOI.[8,26] It has been reported that the DMI can generate noncoplanar/noncollinear spin textures and skyrmions in some specific materials.[27] This proposal is in agreement with the observation of the THE in our samples. The mechanism of the THE is attributed to the Berry phase in real space due to the noncoplanar spin structure.[28,29] Their spin moments would be parallel aligned with an increasing magnetic field, thus depressing the Berry phase, which in turn decreases the THE resistance contribution and results in the formation of the R_{xy} peaks, as observed in our samples. The noncoplanar spin texture proposed also could

DOI: 10.1021/acsami.7b00150
ACS Appl. Mater. Interfaces 2017, 9, 3201−3207

explain the spin-glass-like behaviors observed in this paper based on the Kawamura mechanism,[24,30] whose essential point is that noncoplanar spin configurations introduce spin fluctuations that lead to a spin-glass-like state.[12] The mechanism has been well validated by Monte Carlo simulations.[30,20] Third, the abnormal magnetic and magneto-transport behavior is weakened with the increase of the SIO-thickness, indicating that the interfacial DMI strength is suppressed due to the increased thickness of the SIO layer. This can be explained as follows. The DMI strength is proportional to the spin−orbit interaction strength.[31] At heterostructure interfaces, the spin−orbit interaction strength decreases as the thickness of the layers of the heterostructures increases due to the decreased potential gradient across the interface.[32,33] It is unfortunate that we cannot quantitatively extract the strength of the interfacial Dzyaloshinskii−Moriya interaction and directly observe the interfacial noncoplanar spin texture in our samples. We envision that this work stimulates research to directly image the interfacial spin structure in SRO/SIO superlattices using the Brillouin light scattering technique or the resonant neutron scattering method.[8]

The tendency SL 4/5 > SL 4/13 > SL 4/10 of $M(t)/M(0)$ shown in Figure 2c depends on two factors in our samples, the non-coplanar spin texture depth (proportional to the volume of the non-coplanar spin texture) and the rotation angle of the spin under an external magnetic field before the relaxation measurement. They inversely depend on the interfacial DMI, therefore inversely depend on the SIO layer thickness. A simple tendency of $M(t)/M(0)$ is consequently unexpected. Under particular conditions, the tendency of SL 4/5 > SL 4/13 > SL 4/10 is possible. However, it should be emphasized that, without a specific interpretation, this feature does not influence our analyses and conclusions.

V. CONCLUSION

In summary, we have fabricated $SrRuO_3/SrIrO_3$ superlattices and characterized their magnetic and electron transport behaviors. $SrIrO_3$ layer thickness-dependent spin-glass-like behaviors and topological Hall effect were observed. The spin relaxation dynamics follows the modified Stretched function model, which describes a system with the coexistence of spin-glass textures and a ferromagnetic background. Our work experimentally displays that an interfacial Dzyaloshinskii−Moriya interaction can be induced at the heterostructures constructed with $SrIrO_3$ and other functional perovskite oxides, thereby generating versatile novel physics in these heterostructures. This study expands the research area of the current extensively investigated strong SOI 5d transition metal oxides and potentially triggers further theoretical and experimental investigations in such systems, leading to a better understanding of the complex interactions of SOI and other energy degrees. This work also paves a way for the design of potential oxide spintronics devices with specific functions.

■ ASSOCIATED CONTENT

Supporting Information

The Supporting Information is available free of charge on the ACS Publications website at DOI: 10.1021/acsami.7b00150.

Two energy level model of the R_{ZFC} and R_{FC} magnetization relaxation measurement routes; XRD of the samples; details of the magnetization relaxation dynamic model and analyses; details of the electronic transport data and analyses; and magnetization of a 4 nm thick single layer $SrIrO_3$ film (PDF)

■ AUTHOR INFORMATION

Corresponding Authors

*E-mail: allen.zhang.ly@gmail.com.

*E-mail: ybchen@nju.edu.cn.

ORCID

Lunyong Zhang: 0000-0002-1193-5966

Author Contributions

B.P. and L.Z. contributed equally to this work.

Notes

The authors declare no competing financial interest.

■ ACKNOWLEDGMENTS

We would like to thank Professor Di Wu and Dr Binbin Zhang of Nanjing University for the enlightening discussions. We would like to acknowledge the financial support from the National Natural Science Foundation of China (51402149, 51472112, 11374140, 11374149, 11004094, 11134006, 11474150, 11174127, and U1432112), the Major State Basic Research Development Program of China (973 Program) (2015CB921203, 2013CB632702), and the Fundamental Research Funds for the Central Universities (20620140630)

■ REFERENCES

(1) Kim, B. J.; Jin, H.; Moon, S. J.; Kim, J. Y.; Park, B. G.; Leem, C. S.; Yu, J.; Noh, T. W.; Kim, C.; Oh, S. J.; Park, J. H.; Durairaj, V.; Cao, G.; Rotenberg, E. Novel J_{eff} = 1/2 Mott State Induced by Relativistic Spin-Orbit Coupling in Sr_2IrO_4. *Phys. Rev. Lett.* **2008**, *101* (7), 076402.

(2) Carter, J.-M.; Shankar, V. V.; Zeb, M. A.; Kee, H.-Y. Semimetal and Topological Insulator in Perovskite Iridates. *Phys. Rev. B: Condens. Matter Mater. Phys.* **2012**, *85* (11), 115105.

(3) Chen, Y.; Lu, Y.-M.; Kee, H.-Y. Topological crystalline metal in orthorhombic perovskite iridates. *Nat. Commun.* **2015**, *6*, 6593.

(4) Yi, D.; Liu, J.; Hsu, S.-L.; Zhang, L.; Choi, Y.; Kim, J.-W.; Chen, Z.; Clarkson, J. D.; Serrao, C. R.; Arenholz, E.; et al. Atomic-scale control of magnetic anisotropy via novel spin−orbit coupling effect in $La_{2/3}Sr_{1/3}MnO_3/SrIrO_3$ superlattices. *Proc. Natl. Acad. Sci. U. S. A.* **2016**, *113* (23), 6397−6402.

(5) Matsuno, J.; Ihara, K.; Yamamura, S.; Wadati, H.; Ishii, K.; Shankar, V. V.; Kee, H.-Y.; Takagi, H. Engineering a Spin-Orbital Magnetic Insulator by Tailoring Superlattices. *Phys. Rev. Lett.* **2015**, *114* (24), 247209.

(6) Zhang, L.; Wu, H.-Y.; Zhou, J.; Wu, F.-X.; Chen, Y. B.; Yao, S.-H.; Zhang, S.-T.; Chen, Y.-F. TEM study of $SrIrO_3$ thin films with various thicknesses grown on (001) $SrTiO_3$ substrates synthesized by pulsed laser deposition. *Appl. Surf. Sci.* **2013**, *280* (0), 282−286.

(7) Wu, F. X.; Zhou, J.; Zhang, L. Y.; Chen, Y. B.; Zhang, S. T.; Gu, Z. B.; Yao, S. H.; Chen, Y. F. Metal−insulator transition in $SrIrO_3$ with strong spin−orbit interaction. *J. Phys.: Condens. Matter* **2013**, *25* (12), 125604.

(8) Cho, J.; Kim, N.-H.; Lee, S.; Kim, J.-S.; Lavrijsen, R.; Solignac, A.; Yin, Y.; Han, D.-S.; van Hoof, N. J. J.; Swagten, H. J. M.; Koopmans, B.; You, C.-Y. Thickness dependence of the interfacial Dzyaloshinskii−Moriya interaction in inversion symmetry broken systems. *Nat. Commun.* **2015**, *6*, 7635.

(9) Bode, M.; Heide, M.; von Bergmann, K.; Ferriani, P.; Heinze, S.; Bihlmayer, G.; Kubetzka, A.; Pietzsch, O.; Blugel, S.; Wiesendanger, R. Chiral magnetic order at surfaces driven by inversion asymmetry. *Nature* **2007**, *447* (7141), 190−193.

(10) Biswas, A.; Rossen, P. B.; Yang, C. H.; Siemons, W.; Jung, M. H.; Yang, I. K.; Ramesh, R.; Jeong, Y. H. Universal Ti-rich termination of atomically flat $SrTiO_3$ (001), (110), and (111) surfaces. *Appl. Phys. Lett.* **2011**, *98* (5), 051904−3.

DOI: 10.1021/acsami.7b00150
ACS Appl. Mater. Interfaces 2017, 9, 3201−3207

(11) Bohra, M.; Wu, C. P.; Yeh, H. J.; Cheng, Y. H.; Peng, C. C.; Chou, H. Role of Ru vacancies in the magnetism of strain relaxed SrRuO3 films on SrTiO3 substrates. *J. Appl. Phys.* **2011**, *109* (7), 07D728.
(12) Mydosh, J. A. *Spin Glasses: An Experimental Introduction*; Taylor and Francis, 1993.
(13) Mitchler, P. D.; Roshko, R. M.; Ruan, W. Non-equilibrium relaxation dynamics in the spin glass and ferromagnetic phases of CrFe. *Philos. Mag. B* **1993**, *68* (4), 539−550.
(14) Sinha, G.; Chatterjee, R.; Uehara, M.; Majumdar, A. K. Relaxation of thermo-remanent magnetization in different magnetic phases of Fe-rich γ-FeNiCr alloys. *J. Magn. Magn. Mater.* **1996**, *164* (3), 345−356.
(15) Gabay, M.; Toulouse, G. Coexistence of Spin-Glass and Ferromagnetic Orderings. *Phys. Rev. Lett.* **1981**, *47* (3), 201−204.
(16) Gan, Q.; Rao, R. A.; Eom, C. B.; Garrett, J. L.; Lee, M. Direct measurement of strain effects on magnetic and electrical properties of epitaxial $SrRuO_3$ thin films. *Appl. Phys. Lett.* **1998**, *72* (8), 978−980.
(17) Terai, K.; Ohnishi, T.; Lippmaa, M.; Koinuma, H.; Kawasaki, M. Magnetic Properties of Strain-Controlled $SrRuO_3$ Thin Films. *Jpn. J. Appl. Phys.* **2004**, *43* (2A), L227.
(18) Koster, G.; Klein, L.; Siemons, W.; Rijnders, G.; Dodge, J. S.; Eom, C.-B.; Blank, D. H. A.; Beasley, M. R. Structure, physical properties, and applications of $SrRuO_3$ thin films. *Rev. Mod. Phys.* **2012**, *84* (1), 253−298.
(19) Neubauer, A.; Pfleiderer, C.; Binz, B.; Rosch, A.; Ritz, R.; Niklowitz, P. G.; Böni, P. Topological Hall Effect in the A Phase of MnSi. *Phys. Rev. Lett.* **2009**, *102* (18), 186602.
(20) Lee, M.; Kang, W.; Onose, Y.; Tokura, Y.; Ong, N. P. Unusual Hall Effect Anomaly in MnSi under Pressure. *Phys. Rev. Lett.* **2009**, *102* (18), 186601.
(21) Ohuchi, Y.; Kozuka, Y.; Uchida, M.; Ueno, K.; Tsukazaki, A.; Kawasaki, M. Topological Hall effect in thin films of the Heisenberg ferromagnet EuO. *Phys. Rev. B: Condens. Matter Mater. Phys.* **2015**, *91* (24), 245115.
(22) Yasuda, K.; Wakatsuki, R.; Morimoto, T.; Yoshimi, R.; Tsukazaki, A.; Takahashi, K. S.; Ezawa, M.; Kawasaki, M.; Nagaosa, N.; Tokura, Y. Geometric Hall effects in topological insulator heterostructures. *Nat. Phys.* **2016**, *12* (6), 555−559.
(23) Bern, F.; Ziese, M.; Setzer, A.; Pippel, E.; Hesse, D.; Vrejoiu, I. Structural, magnetic and electrical properties of $SrRuO_3$ films and $SrRuO_3/SrTiO_3$ superlattices. *J. Phys.: Condens. Matter* **2013**, *25* (49), 496003.
(24) Kawamura, H. Chiral ordering in Heisenberg spin glasses in two and three dimensions. *Phys. Rev. Lett.* **1992**, *68* (25), 3785−3788.
(25) Taniguchi, T.; Yamanaka, K.; Sumioka, H.; Yamazaki, T.; Tabata, Y.; Kawarazaki, S. Direct Observation of Chiral Susceptibility in the Canonical Spin Glass AuFe. *Phys. Rev. Lett.* **2004**, *93* (24), 246605.
(26) Fert, A.; Cros, V.; Sampaio, J. Skyrmions on the track. *Nat. Nanotechnol.* **2013**, *8* (3), 152−156.
(27) Seki, S.; Mochizuki, M. *Skyrmions in Magnetic Materials*; Springer, 2015.
(28) Tatara, G.; Kawamura, H. Chirality-Driven Anomalous Hall Effect in Weak Coupling Regime. *J. Phys. Soc. Jpn.* **2002**, *71* (11), 2613−2616.
(29) Kawamura, H. Anomalous Hall Effect as a Probe of the Chiral Order in Spin Glasses. *Phys. Rev. Lett.* **2003**, *90* (4), 047202.
(30) Kawamura, H. Chirality Scenario of the Spin-Glass Ordering. *J. Phys. Soc. Jpn.* **2010**, *79* (1), 011007.
(31) Moriya, T. Anisotropic Superexchange Interaction and Weak Ferromagnetism. *Phys. Rev.* **1960**, *120* (1), 91−98.
(32) Lee, T. Y.; Chang, J.; Hickey, M. C.; Koo, H. C.; Kim, H.-j.; Han, S. H.; Moodera, J. S. Quantum well thickness dependence of Rashba spin−orbit coupling in the InAs/InGaAs heterostructure. *Appl. Phys. Lett.* **2011**, *98* (20), 202504.
(33) Li, J.; Chang, K.; Hai, G. Q.; Chan, K. S. Anomalous Rashba spin-orbit interaction in InAs/GaSb quantum wells. *Appl. Phys. Lett.* **2008**, *92* (15), 152107.
(34) Matsuno, J.; Ogawa, N.; Yasuda, K.; Kagawa, F.; Koshibae, W.; Nagaosa, N.; Tokura, Y.; Kawasaki, M. Interface-driven topological Hall effect in $SrRuO_3$-$SrIrO_3$ bilayer. *Sci. Adv.* **2016**, *2* (7), e1600304.

NOTE ADDED IN PROOF

During the polishing of this paper, we became aware of ref 34, which reported the topological Hall effect in bilayer SRO/SIO and showed the SRO thickness dependence of the THE; simultaneously, it proposed that skyrmions are formed at the SRO side of the SRO/SIO interface based on a multilayer system Hamiltonian simulation. Our work studies SRO/SIO superlattices and reports the SIO layer thickness dependence of the THE; in addition, it provides an in-depth demonstration of the magnetic behaviors and their SIO layer thickness dependence and reveals the connection between the THE and the magnetic structure.

DOI: 10.1021/acsami.7b00150
ACS Appl. Mater. Interfaces 2017, 9, 3201−3207

Supporting materials for

Spin-glass-like behavior and topological Hall effect in $SrRuO_3/SrIrO_3$ superlattices for oxide spintronics applications

Bin Pang[1], Lunyong Zhang[1,2*], Y.B Chen[3*], Jian Zhou[1] , Shuhua Yao[1], Shantao Zhang[1], Yanfeng Chen[1]

1. *National Laboratory of Solid State Microstructures & Department of Materials Science and Engineering, Nanjing University, Nanjing 210093, China*
2. *Max Planck POSTECH Center for Complex Phase Materials, Max Planck POSTECH/Korea Research Initiative (MPK), Gyeongbuk 376-73, Korea*
3. *National Laboratory of Solid State Microstructures & Department of Physics, Nanjing University, 210093 Nanjing, China*

** Corresponding authors:*

Lunyong Zhang allen.zhang.ly@gmail.com and Y.B Chen ybchen@nju.edu.cn

1. Two energy level model of R_{ZFC} and R_{FC} magnetization relaxation measurement routes

In the present work, the magnetization relaxation experiments were carried out through two kinds of field routes.

The R_{FC} route: the samples were 0.1T field cooled to the target temperature from room temperature, and then removing the field following collecting the magnetization data. The magnetization relaxation data shown in figure 2c were measured under this route.

The R_{ZFC} route: the samples were first zero field cooled to the target temperature and then kept in an out plane magnetic field of 0.1T for 5 minutes, after that the field was removed the magnetization data were collected. The magnetization relaxation data shown in figure 2d were measured under this route.

We believe the R_{ZFC} route is more powerful to identify the spin glass like state than the R_{FC} route. The reason is discussed as following. Without loss of generality, a two energy states system with spin glass state and long rang magnetic ordering state can be profiled as figure S1. If the system has a background state with FM, the system would not be relaxed no matter after the FC or ZFC because it has been located at the lowest energy background (figure S1 a). If the system has a background state with AFM, relaxation is not expected to be observed since it has been entered the lowest energy background (figure S1 b). Using R_{FC}, when the exchange interaction causing the AFM state is large, so a FC induced spin parallel state is highly unstable, the system will relaxed to the background AFM state instantaneously when the field for FC is removed, so it is not expected to observe distinct relaxation, but when the exchange interaction is relatively waken or due to unavoidable defect in practice, the relaxation would be not instantaneous, so distinct relaxation can be observed (figure S1 c).

If the system is as shown in figure S1 d) with a spin glass background state. Using R_{ZFC}, the system will directly enter the spin glass state during the ZFC, and then the small external field would arouse spin fluctuation and relaxation would be observed after the field is removed. Under $R_{FC,}$ the system possible enter a metastable FM state which cannot relax when the barrier energy E is larger than k_BT (T is temperature). When E is smaller than k_BT, relaxation is expected.

Consequently, when relaxation is observed under the R_{ZFC} route, long range magnetic ordering state is excluded, and spin glass state is most possible. In contrast under the R_{FC} route, AFM state is also possible when observing magnetic relaxation. Whatever, magnetic relaxation is demonstrated in the measurements under both the R_{ZFC} route and the R_{FC} route, therefore we conclude a spin glass like state in our SRO/SIO superlattices.

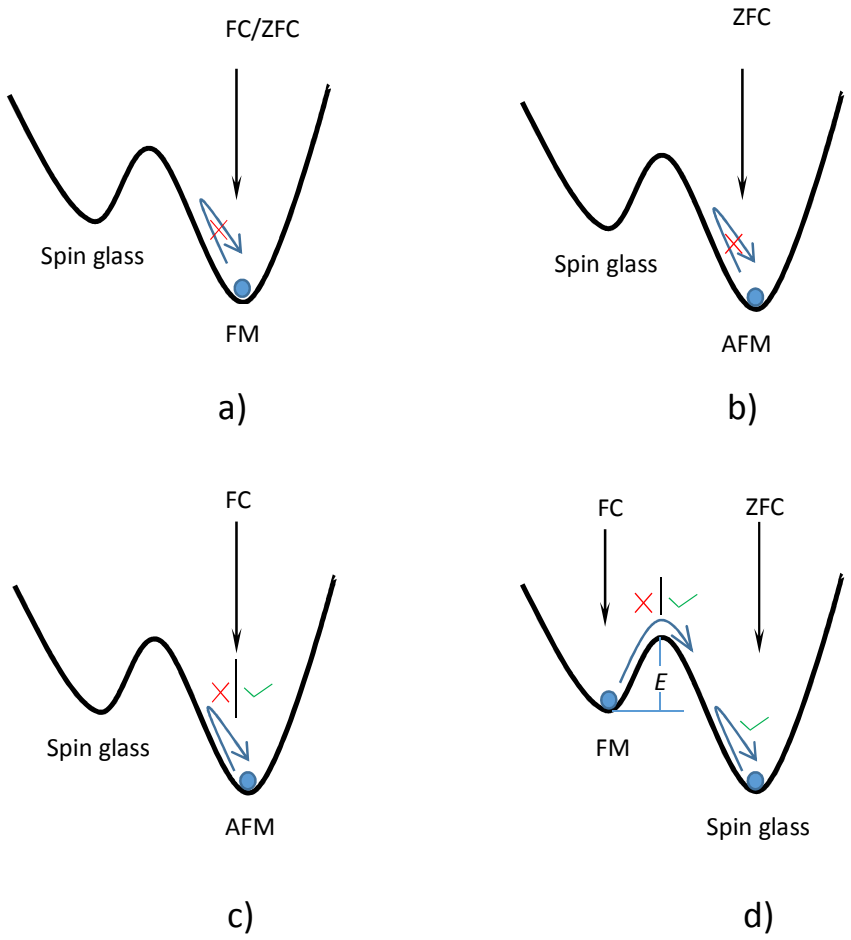

Figure S1 Schematic energy diagram of a two energy states system with spin glass state and long rang magnetic ordering state. The cross symbol notes that the magnetic relaxation is not expected, and tick symbol notes that the magnetic relaxation is expected. *E* is barrier energy.

2. XRD

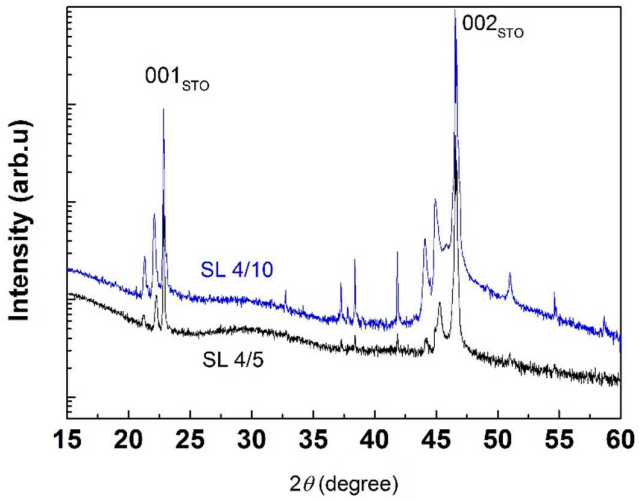

Figure S2 Representative XRD patterns of the samples SL 4/5 and SL 4/10.

3. Magnetization relaxation dynamics

The Stretched function usually adopted in description of relaxation phenomenon could be written as a general format as[1]

$$M(t) = M_0 \exp\left[-\left(\frac{t}{\tau}\right)^{\alpha}\right] \qquad \text{Equation S1}$$

So a linear dependent relation can be obtained as following

$$\ln\left[-\ln\left(\frac{M}{M_0}\right)\right] = \alpha \ln t - \alpha \ln \tau \qquad \text{Equation S2}$$

Figure S3 gives out the relaxation curves transformed according to Eq.S2. Obviously, no linear dependence could be assigned in the whole relaxation time.

The modified Stretched function is written as[2-3]

$$M(t) = M_0 + M_1 \exp\left[-\left(\frac{t}{\tau}\right)^{\alpha}\right] \qquad \text{Equation S3}$$

Which gives out the $M(0)=M_0+M_1$, so for normalized magnetization like we have adopted Eq.S3 is written into

$$M'(t) = \frac{M(t)}{M_0 + M_1}$$
$$= \frac{M_0}{M_0 + M_1} + \frac{M_1}{M_0 + M_1} \exp\left[-\left(\frac{t}{\tau}\right)^{\alpha}\right] \qquad \text{Equation S4}$$
$$= M_0' + M_1' \exp\left[-\left(\frac{t}{\tau}\right)^{\alpha}\right]$$

Table S1 gives out the fitted constants for the relaxation curves in figure 2c and figure 2d using Eq.S4. The fitted values of the exponential constant α for the 10K data of SL 4/5 are in agreement for the R_{ZFC} and R_{FC}, indicating same structure basis in the two relaxation processes.

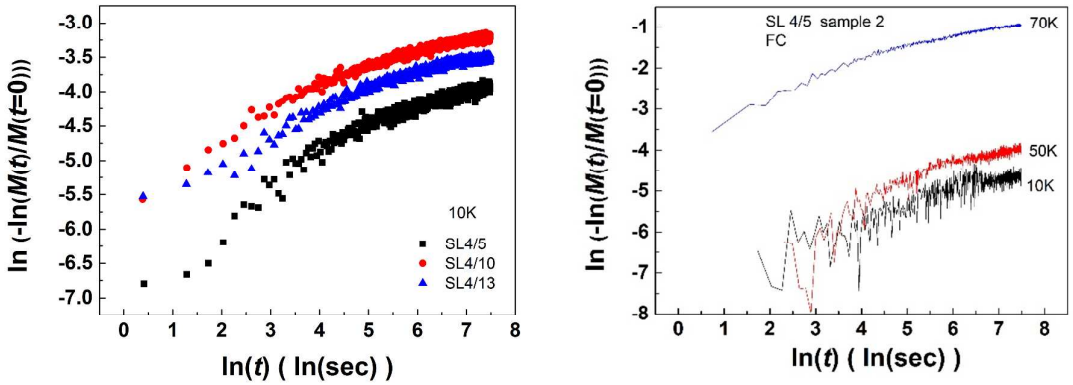

Figure S3 Magnetization relaxation data transformed according to the Stretched function

Table S1 Fitted constant values of magnetization relaxation according to the modified Stretched function model Eq.S5

	M_0'	M_1'	τ	α
Sample	10K (figure 2c)			
SL4/5	0.976	0.024	361.922	0.359
SL4/10	0.957	0.043	155.419	0.391
SL4/13	0.967	0.033	151.903	0.491
Temperature	SL 4/5 sample 2 (figure 2d)			
10K	0.988	0.015	216.068	0.350
50K	0.980	0.020	243.894	0.510
70K	0.636	0.364	202.851	0.376

4. Electronic transport

Figure S4 gives out the temperature dependent resistance of the samples, where resistance kinks indicating the itinerant ferromagnetic transition in $SrRuO_3$ layers are demonstrated. Inset

more clearly shows the transition points T_c, it was shown T_c is decreased with increasing the $SrIrO_3$ layer thickness. The low temperature resistance upturn may come from two contributions, one is the enhanced scattering coming from the spin glass freezing, and another one is owing to the weak localization of carriers. We noted the SIO layer thickness dependence of R': SL4/5<SL4/13<SL4/10. It could be explained as the SIO layer conductance component increases with increasing SIO layer thickness in the superlattice with parallel connection of SIO resistor and SRO resistor, so more and more feature coming from the R' of SIO layer would exhibited in the sample with thicker SIO layer. It is known the R' of SIO film is larger than that of SRO film since SRO is of better metallicity[4-5], for example see figure S5. As for why the R' (SL 4/13) is lower than R' (SL 4/10), we believe that comes from the stronger carrier weak localization in SL 4/10 due to inevitable and difficult controlled defects because weak localization caused resistance increase at low temperature will increase R'. It can be seen the metal transition temperature of SL 4/10 is higher than that of SL 4/13.

Figure S6 shows the Hall resistances of the samples SL 4/10 and SL 4/13. Hysteresis in the temperature regime below T_c is obvious, which is similar to the Hall traces of SL 4/5 shown in the main text. Topological Hall signal could be slightly seen for the sample SL 4/10 at 10K, but no for the SL 4/13.

Figure S7 a) and b) present the magnetoresistances of the samples SL 4/10 and SL 4/13, respectively. Hysteresis was distinctly demonstrated at the temperatures at 2K and 10K. Figure S6 c) and d) give out the differential curves of the MR of the samples at 2K and 10K, the emergent variation of dMB/dB contributed by the recovering of the chiral ordering spin texture, pointed out by the arrows, is only distinct for the sample SL 4/5, indicating the weaken of the chiral ordering spin texture with increasing the SIO layer thickness.

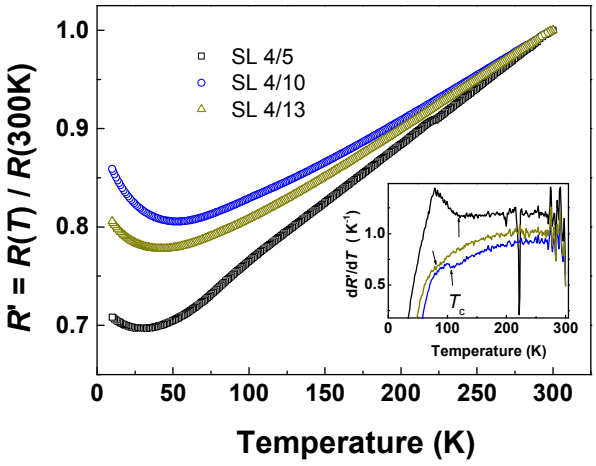

Figure S4 Temperature dependent resistance of the samples. Inset showing the differential of resistance to determine the T_c more distinctly.

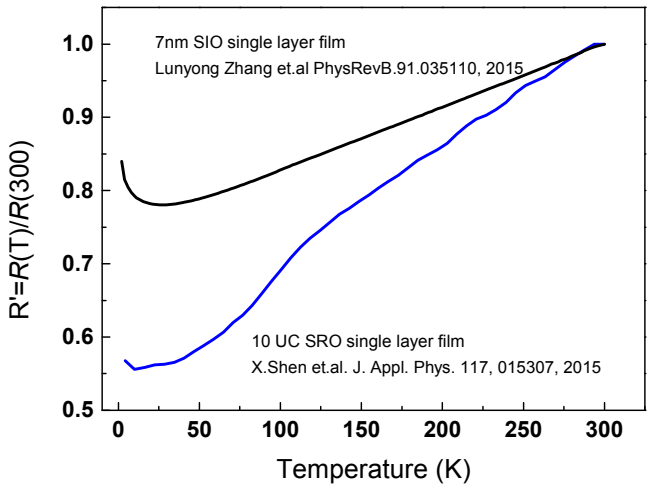

Figure S5 R' of SIO films and SRO films

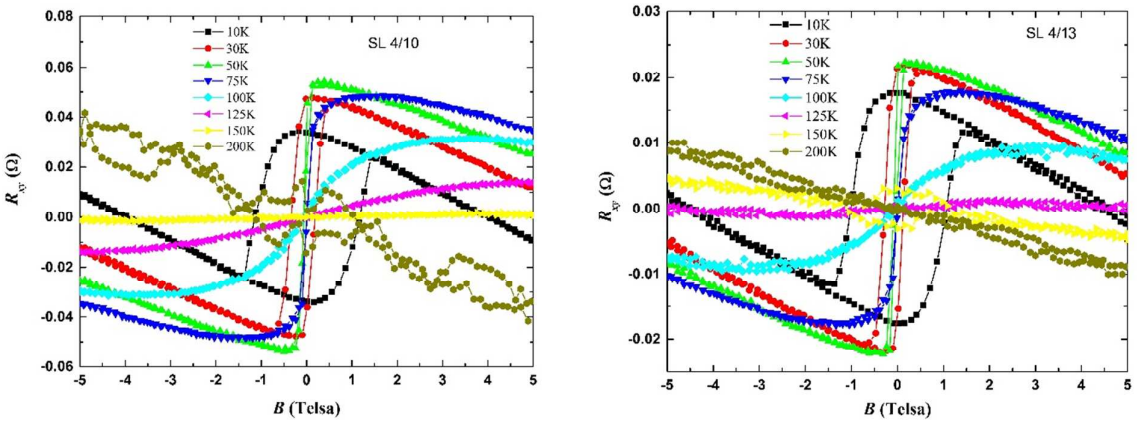

Figure S6 Hall resistance traces of the samples SL 4/10 and SL 4/13

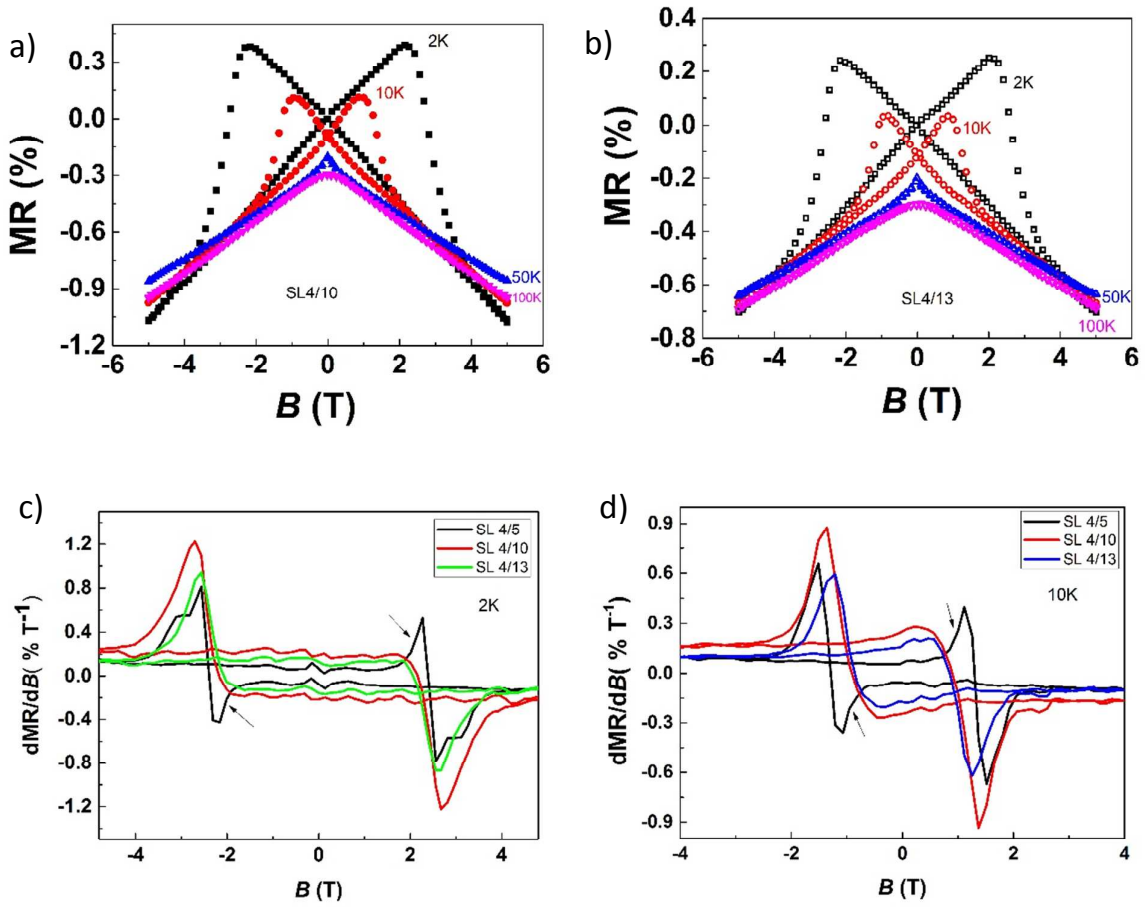

Figure S7 magnetoresistances and their differentials of the samples

5. Magnetization of a 4nm thick single layer $SrIrO_3$ film

The data is quite noise. The magnetization magnitude order is as low as 10^{-6}-10^{-5} emu, which is the limited resolution of our SQUID.

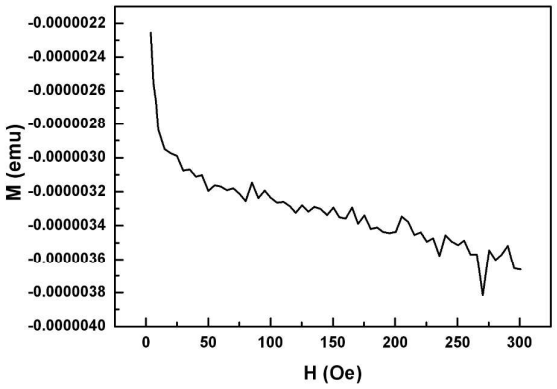

Figure S8 M-T of a 4nm thick single layer $SrIrO_3$ film

References

1. Mydosh, J. A., Spin glasses: An Experimental Introduction. Taylor and Francis: **1993**.
2. Mitchler, P. D.; Roshko, R. M.; Ruan, W., Non-equilibrium relaxation dynamics in the spin glass and ferromagnetic phases of CrFe. *Philos. Mag. B* **1993,** *68* (4), 539-550.
3. Sinha, G.; Chatterjee, R.; Uehara, M.; Majumdar, A. K., Relaxation of thermo-remanent magnetization in different magnetic phases of Fe-rich γ-FeNiCr alloys. *J. Magn. Magn. Mater.* **1996,** *164* (3), 345-356.
4. Shen, X.; Qiu, X.; Su, D.; Zhou, S.; Li, A.; Wu, D., Thickness-dependent metal-insulator transition in epitaxial $SrRuO_3$ ultrathin films. *J. Appl. Phys.* **2015,** *117* (1), 015307.
5. Zhang, L.; Liang, Q.; Xiong, Y.; Zhang, B.; Gao, L.; Li, H.; Chen, Y. B.; Zhou, J.; Zhang, S.; Gu, Z.; Yao, S.; Wang, Z.; Lin, Y.; Chen, Y., Tunable semimetallic state in compressive strained $SrIrO_3$ films revealed by transport behavior. *Phys. Rev. B.* **2015,** *91* (3), 035110.